Paper B

Modelling Demagnetized Permanent Magnet Synchronous Generators using Permeance Network Model with Variable Flux Sources

Sveinung Attestog, Huynh Van Khang, Kjell G. Robbersmyr

This paper has been published as:

S. Attestog, H. Van Khang and K. G. Robbersmyr, "Modelling Demagnetized Permanent Magnet Synchronous Generators using Permeance Network Model with Variable Flux Sources," 2019 22nd International Conference on the Computation of Electromagnetic Fields (COMPUMAG), Paris, France, 2019, pp. 1-4, doi: 10.1109/COMPUMAG 45669.2019.9032791.

B.1 Abstract

The partial demagnetisation in a four-pole 1.5 kW surface mounted permanent-magnet synchronous-generator was modeled by permeance network model (PNM). The results were compared to a 2-D time-stepping finite element analysis (FEA). Both models where simulated in scenarios where one of the magnets where 20 % and 100 % demagnetised and when none of the magnets where demagnetised. The results showed that the proposed PNM with variable magnetic flux sources matched the results of the FEA. The proposed method only need to invers the permeance matrix once before the time simulation, while the traditinal PNM need to invers it in every time step. This make the proposed model less computationally heavy when modeling electrical machines in healthy and faulty conditions, like demagnetisation, short circuit, and static eccentricity. The difference is smaller when modeling dynamic eccentricity, becuase the geometry of the airgap changes over time.

B.2 Introduction

Demagnetisation normally occurs in a permanent-magnet synchronous-generator (PMSG) due to low magnetic flux in high coercivity under high-temperature environments, being the result of poor cooling or overloading [1]. Finding the best indicators for this phenomenon is important for controlling and maintenance of the PMSG. Measured parameters, namely currents, voltages, torques, or output powers, are normally analysed using signal processing techniques in fault diagnosis. This conventional approach is fast, but treats the generator like a black box. Further, run-to-failure tests or seeded faults are often difficult, expensive and infeasible in certain machines. Understanding physical background of a fault allows finding the best measured parameters or fault indicators. Finite element analysis (FEA) has been a useful approach for modelling motors with faults and providing numerical data for testing fault diagnosis algorithm. However, computational burden is the main disadvantage of FEA. Processing powers of modern computers are increasing, but avoiding heavy computation is still important. Further, models and algorithms used in condition monitoring need to be fast to solve, thus a too detailed model is not suited for this purpose. Using permeance network models (PNM) or called magnetic equivalent circuit is a promising solution, but modelling rotation in PNM was identified as a main challenge to be addressed further [2]–[4].

One way to model rotation of the rotor in the PNM is the use of variable resistors in the airgap domain [2]. The nodes connecting between the rotating domain (rotor) and stationary domains (stator) are all connected to one another. Authors in [3] and [4] focused on induction motors and permanent magnet synchronous machines, respectively. The principle is that the permeance in the airgap will change over time when the rotor moves. The permeance depending on rotor position is usually obtained by FEA. If the network has n number of nodes both in the rotor and stator, which are all connected, then $2n^2 + 2n$ entries in the permeance matrix need to be updated, because of the change in rotor position. Another approach is to re-mesh the network in the airgap domain when the rotor moves as detailed in [5], which is almost like a FEA. The permeance matrix

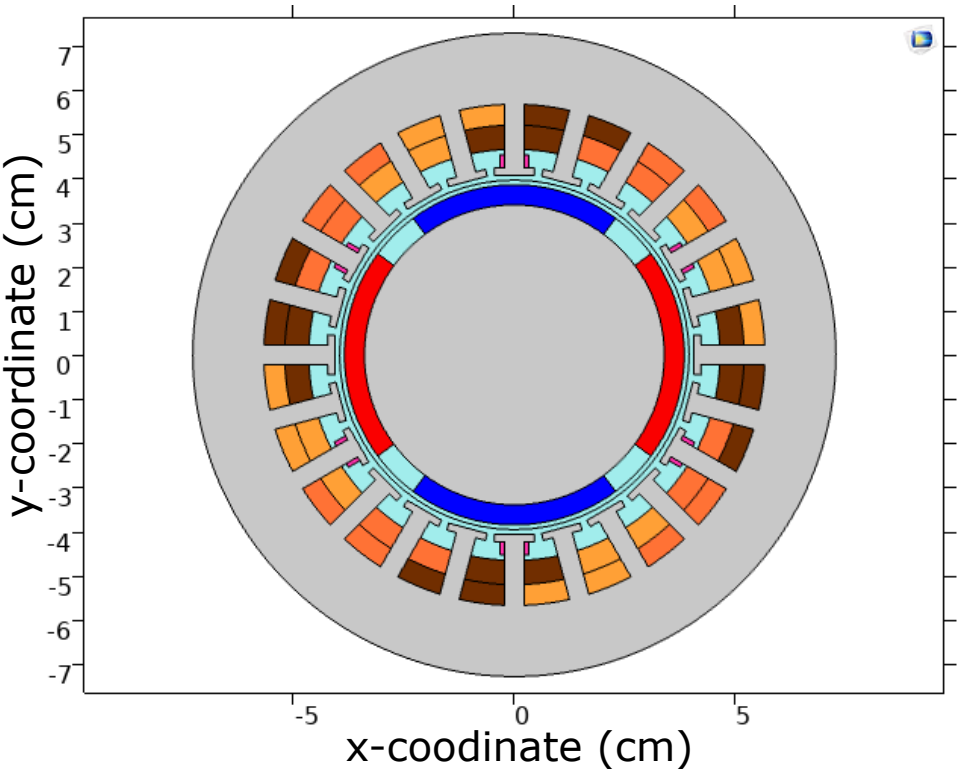

Figure B.1: Model geometry of permanent magnet synchronous generator

need to be inverted in every time step, because of the re-meshing. This is the majority of the computational complexity. Other methods involve hybrid models between PNM and FEA [6].

This work proposes a method to model rotation of the rotor in a PNM. The suggested method involves adjusting the magnetic flux sources representing the magnets and changing their direction over time. This method would be less complex as compared to the existing methods because it does not require any change of the entries in the permeance matrix over time due to the rotation of the rotor. The time depended parameters will be in the vector describing the magnetic flux sources in the network. Furthermore, the developed PNM is used to model a PMSG under healthy and demagnetised conditions.

B.3 Permeance Network Model

This section will describe and explain the proposed method for describing the PNM with variable magnetic flux sources. The geometry of a four-pole 1.5 kW surface mounted PMSG with double layer distributed windings is shown in Figure B.1, which is also used in the FEA for a comparative study.

B.3.1 Reluctance and Permeance

Permeance is the inverse of reluctance. The PMSG in Figure B.1 is subdivided into smaller elements called flux tubes. The general equation for computing the reluctance of the flux tube connected between nodes i and j is:

$$\mathcal{R} = \int_i^j \frac{1}{\mu(l)\mathrm{A}(l)} dl, \tag{B.1}$$

where μ is the permeability and $A(l)$ is the cross-sectional area along length l. The equations for the permeance of a few specific geometries are given in [7]. The permeance for stator teeth was computed by the equations for box shape flux tubes while the remaining flux tubes are calculated by the equations for trapezoids, which is different depending on direction of the flux [7].

B.3.2 Magnetic Flux Sources

The equivalent circuit of a permanent magnet or other sources of magnetic motive force (MMF) is a voltage source connected in series with a reluctance. A sketch of the equivalent circuit is shown in Figure B.5. This circuit can be replaced with a current source connected parallel with a reluctance [5] as shown in Figure B.3.

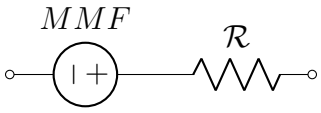

Figure B.2: Equivalent circuit of a magnetic motive force source

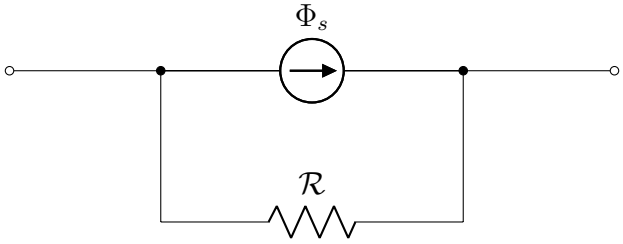

Figure B.3: Equivalent circuit of a magnet flux source

The relation between MMF and Φ_s is given by

$$\Phi_s = \frac{\mathrm{MMF}}{\mathcal{R}}. \tag{B.2}$$

The MMF sources induced by the phase currents I_a, I_b and I_c are computed by

$$\mathrm{MMF}_{\mathbf{Coil}} = N_a I_a + N_b I_b + N_c I_c, \tag{B.3}$$

where $\boldsymbol{N_a}$, $\boldsymbol{N_b}$ and $\boldsymbol{N_c}$ are vectors describing the number of turns in each stator slot and direction of the windings of phase a, b and c, respectively. The first entry of $\mathbf{MMF}_{\mathbf{Coil}}$ is the MMF source induced by the phase currents in the windings of stator slot number 1.

The value of Φ_s for a permanent magnet is equal to the product of its coercive force and height [5]. A second approach is to select the magnetic flux density induced by the magnet and multiply by the cross-sectional area of the flux tube in the PNM containing

the magnet. The flux sources describing the magnets of a healthy permanent magnet machine is defined as

$$\Phi_{mag}(\theta) = \begin{cases} \Phi_s & \text{if } \theta - \theta_{ref} \in [0, \frac{5\pi}{12}] \cup [\pi, \frac{17\pi}{12}] \\ -\Phi_s & \text{if } \theta - \theta_{ref} \in [\frac{\pi}{2}, \frac{11\pi}{12}] \cup [\frac{3\pi}{2}, \frac{23\pi}{12}] \\ 0 & \text{else} \end{cases} \tag{B.4}$$

The reference angle θ_{ref} is with respect to the position of the stator teeth in the model. The position of the rotor needs to have a value between 0 and 2π. Alternatively, (B.4) can be replaced by a single continuous equation obtained from Fourier transform, which has the similar shape. If (B.4) is used, sudden jumps in the estimated flux density over time will occur. Demagnetisation can be modelled by decreasing the magnitude of the magnetic flux density from portions of the magnet.

B.3.3 Model Setup

Magnetic flux sources are used instead of MMF sources, because this reduces the size of the matrix describing the network [5]. The governing equation of the PNM is

$$\boldsymbol{\mathcal{P}} \boldsymbol{F_m} = \boldsymbol{\Phi_s}, \tag{B.5}$$

where

$$\boldsymbol{\mathcal{P}} = \begin{bmatrix} \mathcal{P}(1,1) & \mathcal{P}(1,2) & \cdots & \mathcal{P}(1,n) \\ \mathcal{P}(2,1) & \mathcal{P}(2,2) & \cdots & \mathcal{P}(2,n) \\ \vdots & \vdots & \ddots & \vdots \\ \mathcal{P}(n,1) & \mathcal{P}(n,2) & \cdots & \mathcal{P}(n,n) \end{bmatrix}, \tag{B.6}$$

$$\boldsymbol{F_m} = \begin{bmatrix} F_m(1) \\ F_m(2) \\ \vdots \\ F_m(n) \end{bmatrix} \tag{B.7}$$

and

$$\boldsymbol{\Phi_s} = \begin{bmatrix} \Phi_s(1) \\ \Phi_s(2) \\ \vdots \\ \Phi_s(n) \end{bmatrix}. \tag{B.8}$$

The diagonal entries in permanence matrix $\boldsymbol{\mathcal{P}}$ are the sum of permeances connected to a node and the remain entries are the permeance between 2 different nodes multiplied by -1. In the case of a PNM with n number of nodes and m number of magnetic flux sources, the size of $\boldsymbol{\mathcal{P}}$ is $n \times n$. If the magnets and the MMF induced by the phase currents was represented by the equivalent circuit in Figure B.2, the size of the matrix describing the network would increase to $(n+m) \times (n+m)$.

Previous papers showed how rotation could be modelled by variable airgap permeances [2] or re-meshing the network in the airgap [5]. These strategies must change the entries

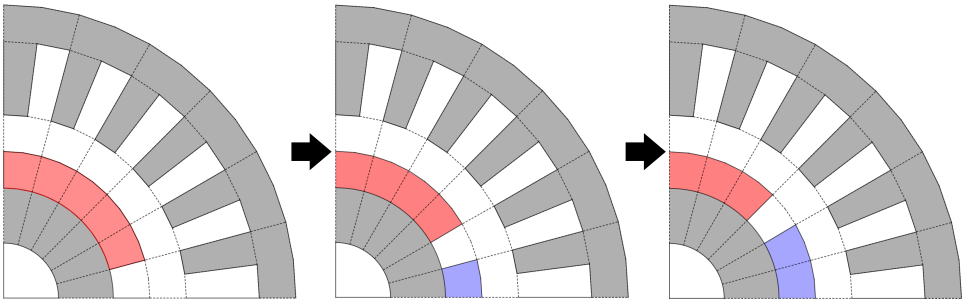

Figure B.4: Illustration of moving rotor (counter clockwise rotation)

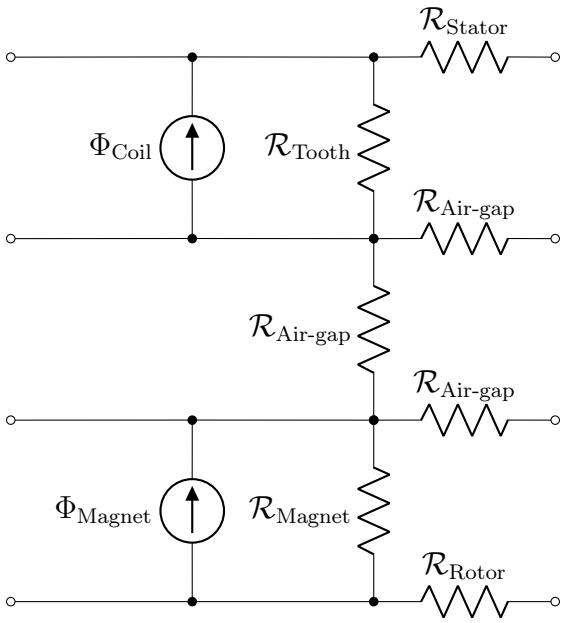

Figure B.5: Unit equivalent circuit of permeance network

of the permeance matrix and invert it in every time step. It is proposed in this paper to change the direction of flux sources representing the magnets instead. Figure B.4 shows a sketch of a quarter of the motor at different rotor positions. The whole motor geometry is subdivided into 24 sectors. Each of them includes one stator tooth, one stator slot and parts of airgap, magnet, rotor and stator yoke. One of these sections can be described with the magnetic circuit in Figure B.5. Within Figure B.4, the red domain is the North pole with magnetic flux point radially outwards, and the blue domain is the South pole with magnetic flux source pointing radially inwards. The magnetic flux in the source switches between a positive value (North pole) and a negative value (South pole). The flux sources in the domains without magnets between the North and South pole are equal to 0 Wb. Variable magnetic flux sources can mimic the rotation of the rotor, and no entry in the permeance matrix needs to change due to the rotation of the rotor and the matrix only need to be inverted once before the time simulation. The exception is dynamic eccentricity where the geometry of in the airgap change over time.

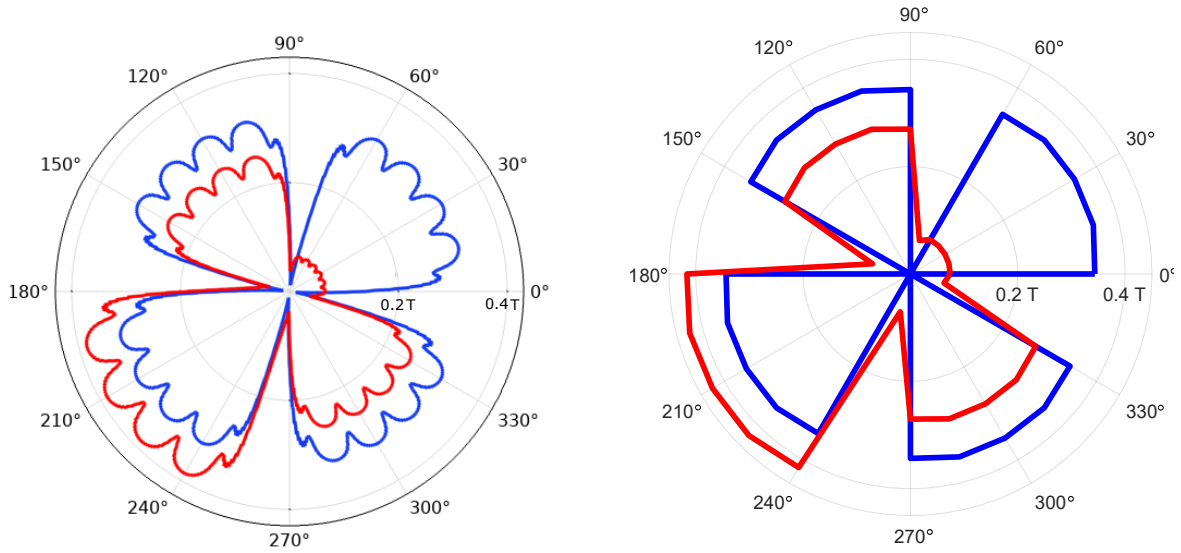

(a) (b)

Figure B.6: Caption place holder

B.4 Results and Discussions

This section will present and discuss the simulation results. A adaptive time-stepping FEA defined by Maxwell's equations were used as a benchmark comparison. The magnets in the FEA were described with the linear model [8]. First simulation was a stationary study with motor speed equal to 0 rpm, and the phase current amplitudes were 0 A. This first simulation generates the initial conditions for time-stepping FEA simulations. The machine was analysed in the generator mode. The terminals were connected to resistive loads of 50 Ω, and the applied prime mover torque was 10 Nm. The achieved steady state speed from the FEA was 1300 rpm and this was set as motor speed in the PNM. Both in the stationary- and time-stepping simulations of the PMSG were modelled in two scenarios, no fault and with one magnet with 20 % demagnetisation and 100 % demagnetisation.

Figure B.6a shows the initial value of magnetic flux density in the middle of the air-gap in the polar coordinate system for a healthy generator (blue) and a demagnetised generator (red). The variation in amplitude in the area covered by magnets is due to variation of air-gap length. It is shown that the magnetic flux density in the middle of the airgap near the demagnetised magnets is much smaller compared to the non-demagnetised magnet. The magnetic flux densities at South poles are also reduced, but increased at the remaining healthy North pole. Therefore, search coils [9] or hall sensors [10] should be installed for monitoring the condition of demagnetisation. The PNM has a coarser resolution but the characteristics the airgap magnetic flux density is still captured in Figure B.6b.

The magnetic flux density from one stator tooth in a healthy case was extracted in the time domain as shown in Figure B.7a, in which the waveforms from the PNM and the FEA have a good agreement. The resulting plots from the PNM have some sudden jumps, but they occur when the the time derivative of the magnetic flux is large. The

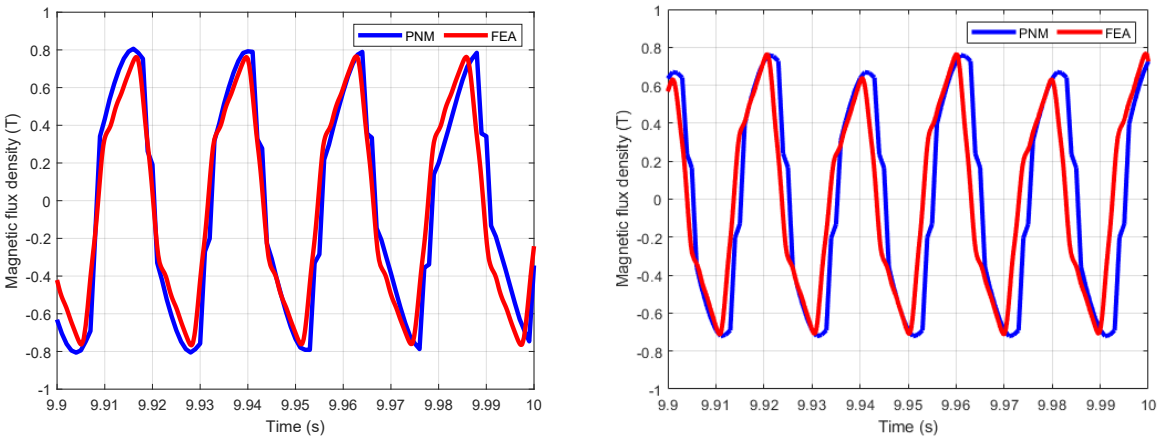

(a) (b)

Figure B.7: Magnetic flux density in stator tooth computed with FEA and PNM with (a) no fault and (b) 20 % demagnetisation on one magnet

magnetic flux sources in magnets are not defined by a continuous function, and at some point the change in magnetic flux density is infinity large. This is not an issue because the network does not include any inductors or capacitor, which would create some dynamic responses. Figure B.7b shows the magnetic flux density through a stator tooth when one of the North poles is demagnetised about 20 %. In other word, the strength of the magnet is reduced to 80 % of original strength. The result from the PNM matches the curve from the FEA.

From simulation time point of view, both PNM and FEA simulated 10 seconds of operation, but the FEA accelerated from 0 to 1300 rpm and the PNM was operating in steady state at a speed of 1300 rpm. The PNM could solve in less than 0.7 s, while the FEA used several hours to complete a 10-second operation. The FEA model used a free triangular mesh with 6609 element with average skewness of 0.78. When the rotor domain moved in each time step, the rotor-mesh did not necessary align with the stator-mesh in the boundary between them. The interpolation across this border boundary is one of the main reason behind the large computational burden. The time step of the FEA decreased when the rotor speed increased, but reducing the tolerance of the solver can improve the computation time.

Saturation was not included in the current model, but the main purpose of this paper was to show how variable magnetic flux sources could represent the rotations of the motor. Saturation can easily be included by setting up a recursive algorithm and iteratively updating the relative permeability of the non-linear material. To achieve this, the first step is to obtain the magnetic flux flowing between the nodes in the network based on an initial guess of the relative permeabilities of the materials defined in the model. Then, the magnetic flux density and magnetic flux intensity are computed, updating of relative permeability and repeating the process until it converges [5].

B.5 Conclusion

This paper proposed a method to model rotation of the rotor in a permeance network model (PNM) with variable magnetic flux sources. This method can lower the computational burden significantly as compared to the traditional models with variable airgap permeances or re-meshing of the network in the airgap. If the centre of rotor does not change over time, it is not necessary to invert the permeance matrix in very time step. The proposed method does not require any special variable permeance function computed in a FEA, which allows more focus on strategic design of the permeance network for accurate computation.

The proposed method was tested on a coarse PNM example, and a comparative study was presented by comparing the results from the proposed model and a FEA, showing that the proposed PNM is able to simulate an PMSG in healthy and faulty condition quickly. The simulated results confirm that the demagnetisation can be detected effectively based on the polar plot of magnetic flux density in the middle of the airgap of the generator by using search coils or hall sensors.

References

[1] N. Nishiyama, H. Uemura, and Y. Honda, "Highly Demagnetization Performance IPMSM Under Hot Environments," *IEEE Transactions on Industry Applications*, vol. 55, no. 1, pp. 265–272, 2019.

[2] C. Delforge and B. Lemaire-Semail, "Induction machine modeling using finite element and permeance network methods," *IEEE Transactions on Magnetics*, vol. 31, no. 3, pp. 2092–2095, 1995.

[3] A. Mahyob, P. Reghem, and G. Barakat, "Permeance Network Modeling of the Stator Winding Faults in Electrical Machines," *IEEE Transactions on Magnetics*, vol. 45, no. 3, pp. 1820–1823, 2009.

[4] D. Faustner, W. Kemmetmüller, and A. Kugi, "Magnetic Equivalent Circuit Modeling of a Saturated Surface-Mounted Permanent Magnet Synchronous Machine," *IFAC-PapersOnLine*, vol. 48, no. 1, pp. 360–365, 2015.

[5] D. Gómez, A. Rodríguez, I. Villar, A. López-de-Heredia, I. Etxeberria-Otadui, and Z. Zhu, "Experimental validation of an enhanced permeance network model for embedded magnet synchronous machines," *Electric Power Systems Research*, vol. 140, pp. 836–845, 2016.

[6] G. Devornique, J. Fontchastagner, D. Netter, and N. Takorabet, "Hybrid Model: Permeance Network and 3-D Finite Element for Modeling Claw-Pole Synchronous Machines," *IEEE Transactions on Magnetics*, vol. 53, no. 6, pp. 1–4, 2017.

[7] M. Zhang, A. Macdonald, K. Tseng, and G. Burt, "Magnetic equivalent circuit modeling for interior permanent magnet synchronous machine under eccentricity fault," *2013 48th International Universities' Power Engineering Conference (UPEC)*, 1–6, Dublin, 2013.

[8] S. Ruoho, E. Dlala, and A. Arkkio, "Comparison of Demagnetization Models for Finite-Element Analysis of Permanent-Magnet Synchronous Machines," *IEEE Transactions on Magnetics*, vol. 43, no. 11, pp. 3964–3968, 2007.

[9] Y. Da, X. Shi, and M. Krishnamurthy, "A New Approach to Fault Diagnostics for Permanent Magnet Synchronous Machines Using Electromagnetic Signature Analysis," *IEEE Transactions on Power Electronics*, vol. 28, no. 8, pp. 4104–4112, 2013.

[10] Y. Park, D. Fernandez, S. B. Lee, *et al.*, "Online Detection of Rotor Eccentricity and Demagnetization Faults in PMSMs Based on Hall-Effect Field Sensor Measurements," *IEEE Transactions on Industry Applications*, vol. 55, no. 3, pp. 2499–2509, 2019.